

Fano Resonances in Majorana Bound States - Quantum Dot Hybrid Systems

Alexander Schuray,¹ Luzie Weithofer,¹ and Patrik Recher^{1,2}

¹*Institut für Mathematische Physik, Technische Universität Braunschweig, D-38106 Braunschweig, Germany*

²*Laboratory for Emerging Nanometrology Braunschweig, D-38106 Braunschweig, Germany*

(Dated: September 4, 2022)

We consider a quantum wire, containing two Majorana bound states (MBS) at its ends that are coupled to a current lead on one side and to a quantum dot (QD) on the other side. Using the method of full counting statistics we calculate the conductance and the zero-frequency noise. Using an effective low-energy model, we analyze in detail the Andreev reflection probability as a function of the various system parameters and show that it exhibits a Fano resonance (FR) line shape in the case of a weakly coupled QD as a function of the QD energy level when the two MBS overlap with an asymmetry parameter that changes sign as the bias voltage is tuned through the MBS overlap energy. The FR is mirrored as function of the QD level energy as long as tunneling to the more distant MBS is negligible. However, if both MBS are coupled to the lead and the QD, the height as well as the asymmetry of the line-shapes cease to respect this symmetry. These two exclusive cases uniquely distinguish the coupling to a MBS from the coupling to a fermionic bound state that is shared between the two MBS. We complement the analysis by employing a discretized one-dimensional p -wave superconductor (Kitaev chain) for the quantum wire and show that the features of the effective low-energy model are robust towards a more complete Hamiltonian and also persist at finite temperature.

I. INTRODUCTION

Transport through Majorana bound states and their manipulation currently attracts a lot of attention both theoretically and experimentally. These particles, first proposed in high energy physics as elementary particles being their own antiparticles by Ettore Majorana [1], could represent the basic building blocks for a topological quantum computer [2, 3]. First experiments have tested their particle-hole symmetry and charge neutrality via a resonance appearing at zero energy [4–8]. Another set of experiments investigate the predicted fractional Josephson effect [9–12] through the missing odd steps in a Shapiro staircase [13, 14]. An important next step is to perform the braiding operations and to show their non-abelian nature [2, 15–22]. The so far most studied systems containing Majorana bound states (MBS) are quantum wire based systems [23–26] having, in the most ideal case, two MBS with one MBS at each end of the wire. In principle, there are several ways in which a splitting of two MBS can be generated. Either direct wave function overlap or charging effects can lead to striking transport features like dominant crossed Andreev reflection [27] or teleportation of charge [28, 29]. In addition a dynamical splitting of two MBS can be induced by the braiding operation in a Corbino geometry topological Josephson junction [30].

Instead of coupling Majorana fermions directly to current leads, one can also employ an additional coupling to other bound states formed e.g. on quantum dots [31–33]. The setup proposed in Ref. [32] with a Majorana wire tunnel coupled to a quantum dot (QD) that is further coupled to a metal lead has very recently also been realized in experiments [34].

Here, we study a setup related to the one used in Ref. [34], but with the important difference that the Majorana wire lies in between the QD and the current lead with no direct coupling between the QD and the lead, see Fig. 1. We show that this setup exhibits Fano resonance (FR) line shapes in conductance (and noise) as a function of the QD level energy ε_D with an asymmetry parameter that can change sign as a function of the bias voltage eV when eV is tuned through the Majorana hybridization energy 2ε . We derive analytical formulas for the resonance energy E_R and the width Γ_F of a corresponding Fano-Beutler formula [35]. Most strikingly, the FR lines are always mirrored when the sign of ε_D is reversed as long as the QD and the lead are only tunnel-coupled to the nearest MBS. This is a direct sign of the particle-hole symmetry of the zero-energy MBS.

However, when the tunnel-coupling to the distant MBS is also finite (see Fig. 3), the symmetry of the conductance (and noise) in ε_D is destroyed, which is a feature that distinguishes between a MBS and a usual fermionic bound state that can be viewed as composed of two MBS. In the latter case, the line shapes of the former mirror-imaged FRs become asymmetric in height, and also can change the sign of the asymmetry parameter. We compare the effective low-energy model with a numerical treatment of a Kitaev chain and find good agreement at low energies. In addition, we also investigate effects of finite temperatures accessible in experiments and find that the main features are still well resolved.

We note that Fano resonances in transport have been known for a long time [35] and appear if a resonant transport path interferes with a structureless transport path. Here, the two transport paths for the injection of a Cooper pair into the grounded superconductor consist of a direct Andreev reflection via the two MBS and a

resonant path where the incoming electron first traverses virtually the quantum wire, visits the QD and then enters the superconducting condensate by reflecting back a hole to the lead. The interference of the two paths can be tuned via the QD level energy. Fano resonances have been discussed previously in the context of Majorana fermions, but only in setups where the QD is coupled directly to the lead, either as a function of bias voltage [36–39] and/or flux through a loop containing the MBS [40–42] and *not* as a function of the QD level energy. Also, the Fano-form of the resonances has been concluded based on a fitting of the conductance line shapes [37], whereas we give analytical expressions for the resonance energy, width and asymmetry of the FR in terms of the model parameters.

The rest of the paper is organized as follows: in Section II, we present the effective low-energy model of the system depicted in Fig. 1(a), present the full counting statistic results for the cumulant generating function (a derivation is given in Appendix A) and the resulting differential conductance and differential noise. In Section III, we discuss the regime of appearance and form of the Fano-resonances as a function of the QD level energy. In Section IV, we discuss a more general setup including also tunnel-couplings to the more distant MBS (see Fig. 3(a)). In Section V, we numerically investigate a Kitaev chain tunnel-coupled to a lead on one side and to a QD on the other, including also possible non-local tunneling amplitudes from the lead to the Kitaev chain and from the QD to the Kitaev chain. In Section VI we give our conclusion. Appendix A gives a derivation of the cumulant generating function in terms of Keldysh Green's functions for the setup and the lead. Appendix B discusses the bias voltage dependence of the conductance for different temperatures.

II. SETUP AND EFFECTIVE MODEL

We consider a setup in which a topologically non-trivial Majorana wire is contacted by a normal conducting lead at one end and tunnel coupled to a QD at the other end, see Fig. 1a). The Majorana edge states of such a wire experience an energy splitting due to their finite wave function overlap $\varepsilon \propto e^{-L/\xi_S}$, where L is the length of the Majorana wire and ξ_S is the superconducting coherence length. A sketch of the setup can be seen in Fig. 1(a). We employ a spinless effective description of the MBS and approximate the QD as a single fermionic level. The

Hamiltonian describing our setup is then given by

$$H = H_L + H_T + H_M + H_{Dot} + H_{TDot} \quad (1)$$

$$H_M = i\varepsilon\gamma_1\gamma_2 \quad (2)$$

$$H_{Dot} = \varepsilon_D d^\dagger d \quad (3)$$

$$H_T = i\gamma_1 [t_1\psi^\dagger(0) + t_1^*\psi(0)] \quad (4)$$

$$H_L = -iv_f \int dx \psi^\dagger(x) \partial_x \psi(x) \quad (5)$$

$$H_{TDot} = i\gamma_2 [t_2 d^\dagger + t_2^* d], \quad (6)$$

where v_f is the Fermi velocity in the normal conducting lead, t_1 is the tunneling amplitude between the the Majorana wire and the lead, t_2 is the tunneling amplitude between the Majorana wire and the quantum dot and ε_D is the energy of the QD level. Here γ_i are the Majorana fermion creation operators, d is the annihilation operator for the quantum dot and $\psi(x)$ is the annihilation operator inside the lead. In order to obtain the transport properties of this setup we use the method of full counting statistics (FCS). The central element of the FCS is the so called cumulant generating function (CGF) [43], which we calculate following the Keldysh technique calculations described in Ref. [44] and summarized in Appendix A. We calculate the CGF in terms of the Keldysh Majorana Green's function

$$\ln \chi(\lambda) = \frac{\mathcal{T}}{2} \int \frac{d\omega}{2\pi} \ln [1 + p(\omega)(e^{-2i\lambda} - 1)n(\omega)n(-\omega) + p(\omega)(e^{2i\lambda} - 1)(n(\omega) - 1)(n(-\omega) - 1)], \quad (7)$$

where $n(\omega) = \frac{1}{1+e^{\beta(\omega-eV)}}$ is the Fermi function in the lead with $\beta = 1/k_B T$ the inverse temperature and \mathcal{T} is a long measurement time. Andreev reflection (which transports 2 electrons) at energy ω occurs with probability $p(\omega)$ and corresponds to the only transport channel. The current and the symmetrized zero-frequency noise in the lead can be calculated by taking the first and the second derivative, respectively of the CGF with respect to the counting field λ . At zero temperature, the differential conductance and differential noise can be presented analytically as

$$\frac{dI}{dV} = \frac{d}{dV} \frac{i}{\mathcal{T}} \frac{\partial}{\partial \lambda} \ln \chi \Big|_{\lambda=0} = \frac{2e^2}{h} p, \quad (8)$$

$$\frac{dP}{dV} = \frac{d}{dV} \frac{-1}{\mathcal{T}} \frac{\partial^2}{\partial \lambda^2} \ln \chi \Big|_{\lambda=0} = \frac{4e^3}{h} p(1-p), \quad (9)$$

where

$$p = \frac{4\Gamma^2(eV)^2}{\left(\frac{4\varepsilon^2(\varepsilon_D^2 - (eV)^2)}{4|t_2|^2 + \varepsilon_D^2 - (eV)^2} - (eV)^2\right)^2 + 4\Gamma^2(eV)^2}, \quad (10)$$

with $\Gamma = 2\pi\rho_0|t_1|^2$ the tunneling rate between the lead and the nearest MBS (γ_1) and where eV is the bias voltage between the lead and the grounded topological superconductor hosting the two MBS. As we are mostly

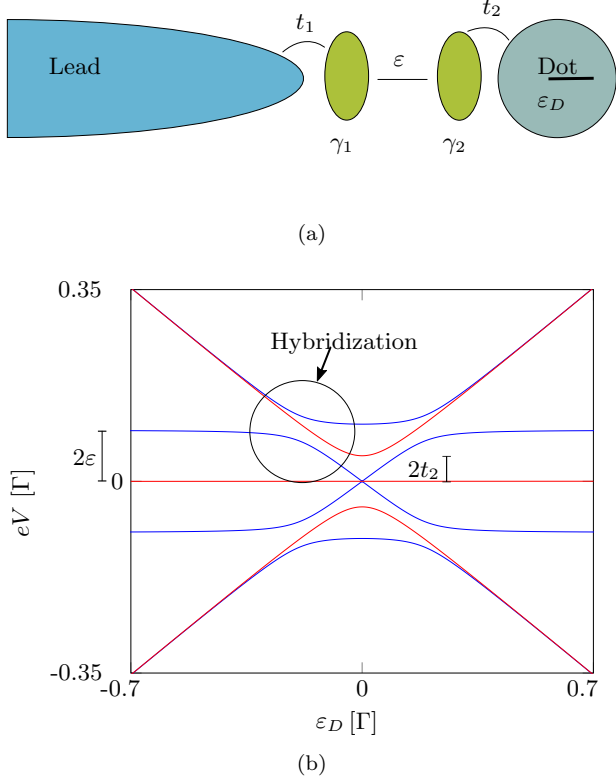


FIG. 1. (a) Schematic sketch of the considered setup, in which two Majorana bound states γ_1 and γ_2 arise in a Kitaev chain. One of them is contacted by a normal conducting lead and the other one with a quantum dot level energy ε_D . The two Majorana bound states experience a splitting ε due to a wave function overlap of the two Majorana fermions. (b) Resonances ($p = 1$, blue) and anti resonances ($p = 0$, red) of the differential conductance in dependence of the bias voltage eV between lead and the Kitaev chain (grounded), and the quantum dot level energy for the parameters $\varepsilon = 0.05\Gamma$ and $t_2 = 0.025\Gamma$. The resonances correspond to the spectrum of the system without the lead. The levels show an avoided crossing if $\varepsilon_D \approx \pm 2\varepsilon$

interested in the dependence of the transport on the QD level energy ε_D it is convenient to rewrite

$$p(\varepsilon_D) = \frac{1}{1 + \frac{q^2(\varepsilon_D^2 - \varepsilon_{D,\max}^2)}{(\varepsilon_D^2 - \varepsilon_{D,0}^2)^2}}, \quad (11)$$

with

$$\begin{aligned} \varepsilon_{D,\max}^2 &= (eV)^2 + \frac{4|t_2|^2 (eV)^2}{(2\varepsilon)^2 - (eV)^2}, \\ \varepsilon_{D,0}^2 &= (eV)^2 - 4|t_2|^2, \\ q^2 &= \frac{(\varepsilon^2 - (eV/2)^2)^2}{\Gamma^2 (eV/2)^2}. \end{aligned} \quad (12)$$

Here, $\varepsilon_D = \varepsilon_{D,\max}$ corresponds to a resonance ($p = 1$), at which every incoming electron is Andreev reflected as a

hole and $\varepsilon_D = \varepsilon_{D,0}$ corresponds to an anti resonance ($p = 0$), where no Andreev reflection is allowed, see Fig. 1b). The parameter q^2 characterizes the Andreev reflection probability without the coupling to the QD. The special point with $\varepsilon_D = eV = 0$ is discussed in Appendix B.

III. FANO RESONANCES

Fano resonances are characterized by a typical asymmetric line shape [45] and appear when a continuous path interferes with a discrete path. In the considered setup, the two paths correspond to a direct Andreev reflection without including the QD, and a path where the incoming electron first traverses the quantum wire, visits the QD and returns to the quantum wire where the electron forms a Cooper pair by emission of a hole into the lead. The second process depends on the QD level energy and corresponds to the discrete path. The interference of both processes leads to a resonance as a function of ε_D .

We intend to describe this resonance in the Andreev reflection probability with the Fano-Beutler formula [35]

$$p_{\text{FB}}(\varepsilon_D) = \frac{1}{1 + q^2} \frac{((\varepsilon_D - E_R)/(2\Gamma_F) + q)^2}{1 + ((\varepsilon_D - E_R)/(2\Gamma_F))^2}, \quad (13)$$

where Γ_F is the width of the FR and E_R is the resonance energy. The parameter q describes the asymmetry of the resonance and its sign determines whether the destructive or constructive interference can be found at smaller energies. It is important to note that this formula only describes one resonance, while we always find two resonances in the considered setup as we will discuss now.

According to Eq. (13), the resonance ($p_{\text{FB}} = 1$) and the anti-resonance ($p_{\text{FB}} = 0$) of a FR as a function of ε_D appear at

$$\varepsilon_D = \varepsilon_{D,\max} \equiv 2\Gamma_F/q + E_R, \quad (14)$$

and at

$$\varepsilon_D = \varepsilon_{D,0} \equiv -2q\Gamma_F + E_R, \quad (15)$$

respectively.

Inserting these into Eq. (11) and considering a small width $|\Gamma_F/E_R| \ll 1$ we can simplify the Andreev reflection probability to

$$\begin{aligned} p(\varepsilon_D) &\approx \left(\frac{1}{1 + q^2} \right) \left(\frac{(\frac{\varepsilon_D - E_R}{2\Gamma_F} + q)^2}{1 + (\frac{\varepsilon_D - E_R}{2\Gamma_F})^2} \right) \\ &\quad \times \left(\frac{(\frac{\varepsilon_D + E_R}{2\Gamma_F} - q)^2}{1 + (\frac{\varepsilon_D + E_R}{2\Gamma_F})^2} \right). \end{aligned} \quad (16)$$

This describes a product of two Fano-Beutler formulas. These two resulting FRs have opposite asymmetry parameters q and opposite resonance energies E_R . We further approximate the Andreev reflection probability in

the limit of large positive E_R/Γ_F compared to q with

$$p(\varepsilon_D) \approx \frac{1}{1+q^2} \frac{(|\varepsilon_D| - E_R + q)^2}{1 + \left(\frac{|\varepsilon_D| - E_R}{2\Gamma_F}\right)^2}. \quad (17)$$

This equation describes two FRs are mirrored at $\varepsilon_D = 0$ and have opposite signs of q and of E_R . If however, the overlap energy ε is smaller than the bias the sign of the asymmetry parameter q of both Fano resonances will Note that the asymmetry parameter $q = \pm((eV/2)^2 - \varepsilon^2)/(\Gamma(eV/2))$ changes sign at both FRs when the bias voltage is tuned through the MBS overlap energy (cf. Fig. 1(b)). Here the $+$ corresponds to the FR at positive ε_D , while $-$ refers to the FR at negative dot level energy. In order to represent the parameters of the Fano-Beutler formula with the parameters of the microscopic model we insert Eq. (14) and Eq. (15) into Eqs. (12) and focus on the FR at positive dot level energy.

$$E_R = 2 \frac{\left(\frac{eV}{2}\right)^2 \Gamma^2 \sqrt{\left(\frac{eV}{2}\right)^2 - t_2^2}}{\left(\frac{eV}{2}\right)^2 \Gamma^2 + \left(\varepsilon^2 - \left(\frac{eV}{2}\right)^2\right)^2} \quad (18)$$

$$+ 2 \frac{\left(\left(\frac{eV}{2}\right)^2 - \varepsilon^2\right)^{3/2} \sqrt{\left(\frac{eV}{2}\right)^2 \left(\left(\frac{eV}{2}\right)^2 - \varepsilon^2 - |t_2|^2\right)}}{\left(\frac{eV}{2}\right)^2 \Gamma^2 + \left(\varepsilon^2 - \left(\frac{eV}{2}\right)^2\right)^2}$$

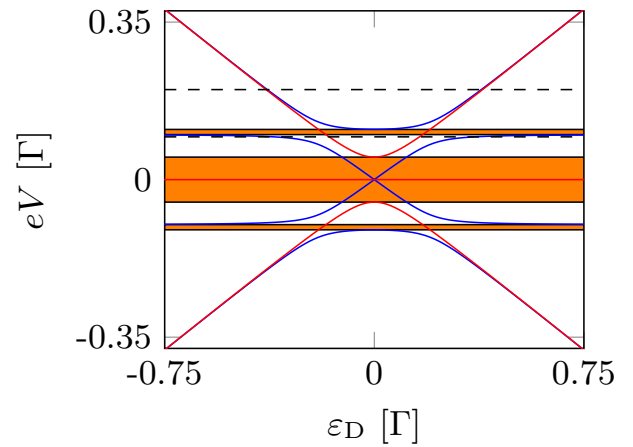
$$\Gamma_F = \frac{\left(\left(\frac{eV}{2}\right)^2 - \varepsilon^2\right) \sqrt{\left(\frac{eV}{2}\right)^2 - t_2^2}}{\left(\frac{eV}{2}\right) \Gamma + \left(\varepsilon^2 - \left(\frac{eV}{2}\right)^2\right) / \left(\left(\frac{eV}{2}\right) \Gamma\right)} \quad (19)$$

$$- \frac{\sqrt{\left(\frac{eV}{2}\right)^2 - \varepsilon^2} \sqrt{\left(\frac{eV}{2}\right)^2 \left(\left(\frac{eV}{2}\right)^2 - \varepsilon^2 - t_2^2\right)}}{\left(\frac{eV}{2}\right) \Gamma + \left(\varepsilon^2 - \left(\frac{eV}{2}\right)^2\right) / \left(\left(\frac{eV}{2}\right) \Gamma\right)}.$$

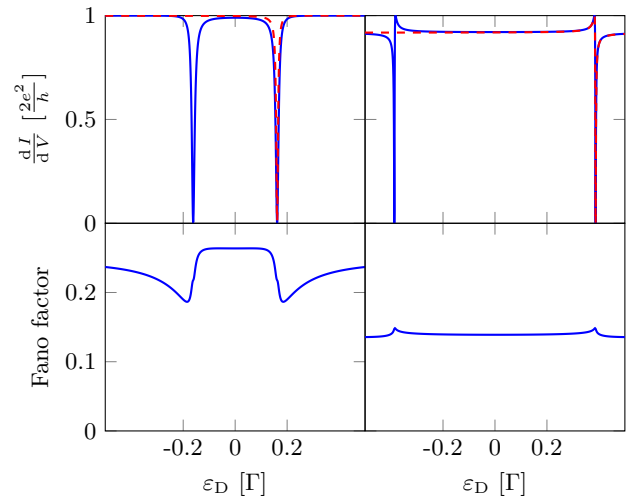
FRs can not be found in a regime where $(eV/2)^2 < |t_2|^2$. In this regime E_R and Γ_F would become complex numbers whereas the differential conductance has to be real valued. Therefore, the description with the Fano formula fails in that regime. Also, in the regime where $\varepsilon < |eV|/2 < \sqrt{|t_2|^2 + \varepsilon^2}$ a description with the Fano-Beutler formula is not possible (cf. Fig. 2(a)).

The assumption of a large resonance energy E_R and small width Γ_F can now be represented with the model parameters and it can be seen that the description with the Fano formula holds for $|t_2| \ll |eV|$. This corresponds to a weakly coupled dot and results in $|E_R| \gg |\Gamma_F|$. This can also be seen in Fig. 2(b), because for a higher bias voltage between lead and topological superconductor the approximation with the FR line shape gets better.

Fig. 2(a) highlights the regime where no FRs appear (orange boxes). This is due to the fact that exclusively either a resonance or anti resonance is crossed when changing ε_D at fixed bias voltage eV . The dashed horizontal lines denote different bias voltages used for the plots in



(a)



(b)

FIG. 2. (a) Resonances and anti resonances in the setup with $\varepsilon = 0.05\Gamma$ and $t_2 = 0.025\Gamma$. The dashed lines correspond to the bias voltages chosen for the plots below. Orange background color marks the parameter space in which no Fano resonances arise. (b) Differential conductance (top) or Fano factor (bottom) vs. dot level for different bias voltages between lead and topological superconductor. The blue line is the exact calculated differential conductance (Fano factor), whereas the red dashed line is the approximation using Eq.(13), where E_R and Γ_F are given by Eq. (18) and Eq. (19) respectively. The noise for these two bias voltages is always sub-poissonian but does not vanish at the conductance resonances which is a sign of a strong energy dependence of the Andreev reflection. The left plots are at $eV = 0.095\Gamma$ and the right plots at $eV = 0.2\Gamma$.

Fig. 2(b). The differential conductance traces are in very good agreement with the deduced Fano form. The dashed lines result from the Fano-Beutler formula Eq. (13) with the parameters expressed in the microscopic parameters of our model Eqs. (18) and Eq. (19). Note that only one resonance is described by the Fano-Beutler formula, the other one is the mirror image with respect to the

line $\varepsilon_D = 0$. Interestingly, the asymmetry parameter q changes sign when the bias voltage is tuned through the Majorana splitting energy 2ε . This gives a direct measure for this energy in terms of a symmetry change in the line shapes of the FR-curves when tuning the bias voltage. Note that the conductance is always quantized at resonances to $2e^2/h$ and is *symmetric* in ε_D . These features are clear signatures of tunneling into *single* MBS, which are zero energy- and particle-hole symmetric-states. The symmetry in the bias voltage (not shown) is more fundamental as it is true for all superconductors. In Fig. 2(b) we in addition show the Fano factor $F = P(V)/eI(V)$ which also shows features at the positions of the FR in conductance. For the chosen parameters in the plots, the noise is always sub-poissonian ($F < 1$). In the next section, we will demonstrate that the symmetry in ε_D is waived when both MBS couple directly to the QD.

IV. NON-MAJORANA FERMIONIC COUPLING

In this section we compare the FRs which arise from an effective model with non-Majorana fermionic couplings, see Fig. 3(a).

Therefore we consider a more general setup in which the normal conducting lead does not only contact one Majorana bound state, but also the second Majorana fermion. The same is true for the connection to the QD. A schematic sketch of this setup can be seen in Figure 3(a). A physical realization of this could be a very short chain, so that the lead not only contacts the first, but also (however much weaker) the last site. The Hamiltonian of this effective setup is

$$\begin{aligned}
 H = & H_L + i\varepsilon\gamma_1\gamma_2 + \varepsilon_D d^\dagger d \\
 & - i\gamma_1 [t_1 \cos(\phi)\psi + t_1 \cos(\phi)\psi^\dagger \\
 & + it_2 \sin(\phi)d - it_2 \sin(\phi)d^\dagger] \\
 & - i\gamma_2 [it_1 \sin(\phi)\psi - it_1 \sin(\phi)\psi^\dagger \\
 & + t_2 \cos(\phi)d + t_2 \cos(\phi)d^\dagger],
 \end{aligned}
 \tag{20}$$

where H_L , γ_i and ψ are the same operators as before and t_1 and t_2 are real valued. In this setup, we can tune between a Majorana-like coupling or a Dirac fermionic coupling by tuning the parameter ϕ , where $\phi = 0$ is the Majorana case as discussed above and $\phi = \frac{\pi}{4}$ corresponds to the case of a single Dirac fermionic site. In between, we have a mixture of Majorana fermionic and Dirac fermionic coupling. The CGF can now be calculated using the same formalism as before and is formally the same as in Eq.(7), however the Andreev reflection probability $p(\omega)$ is different.

By taking the derivative of the CGF with respect to λ we can calculate the differential conductance. It is shown in Figure 3(b) as function of the QD level energy at fixed bias voltage for different ϕ . For $\phi = 0$ we re-

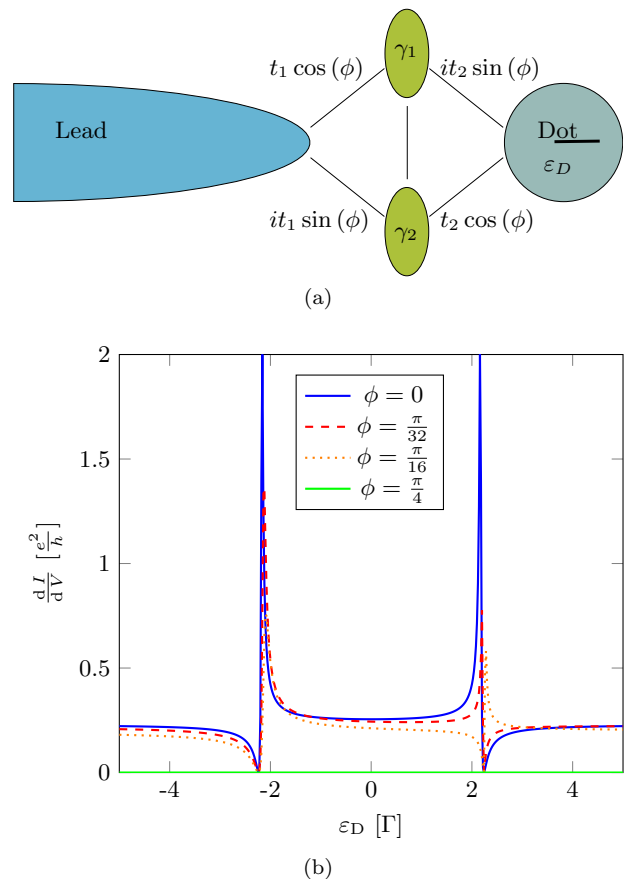


FIG. 3. (a) Sketch of the extended setup. By varying the parameter ϕ we can tune the system from pure Majorana coupling ($\phi = 0$) to pure Dirac fermionic coupling ($\phi = \frac{\pi}{4}$), in order to find unique signatures of pure Majorana fermionic coupling. (b) Differential conductance in the extended setup for different ϕ . In the Majorana coupling case $\phi = 0$ the Fano resonances are quantized and are mirrored at $\varepsilon_D = 0$ due to the real valued properties of the Majorana fermion. For $0 < \phi < \frac{\pi}{4}$ the resonances are no longer quantized and the peaks are no longer symmetric. Parameters are $eV = 3\Gamma$, $|t_2| = \Gamma$, $\varepsilon = 0.4\Gamma$.

duce the results which we have discussed before, while in the $\phi = \frac{\pi}{4}$ case the transport into the superconductor is completely blocked. The case of $0 < \phi < \frac{\pi}{4}$ is more interesting for us. We can clearly see that the resonance peaks of the two arising FRs are no longer quantized and even have a different heights for $\text{sign}(\varepsilon_D) = \pm 1$. We can further tune the system into a regime where the sign of the asymmetry parameters of the two FRs no longer have opposite signs as it is always the case in the Majorana fermionic coupling limit ($\phi = 0$). This is due to the fact that a non-Majorana fermionic level no longer couples to electrons and holes the same, which ends up with a different behaviour for positive and negative dot level energies. In Fig. 4 we present the differential conductance as a function of ε_D and eV and for $\phi = 0.4$. We clearly see that the conductance traces become asymmetric in the

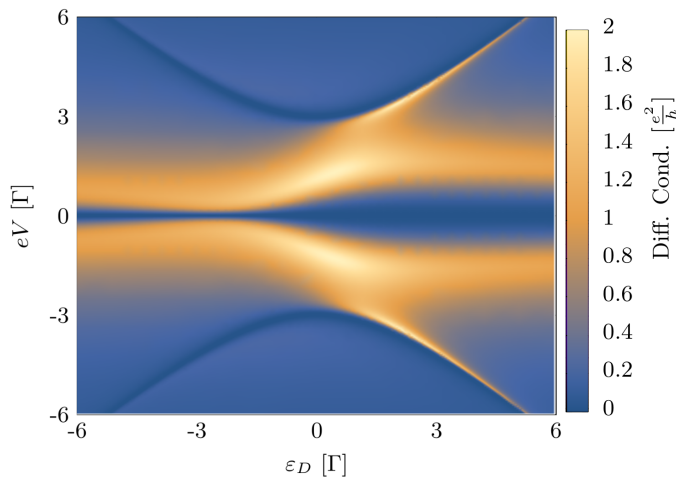


FIG. 4. (a) Differential conductance as function of dot level and bias voltage for non-Majorana fermionic couplings with $\phi = 0.4$, $\varepsilon = 0.5\Gamma$, $|t_2| = 1.5\Gamma$. The maxima of the differential conductance correspond to the eigenenergies of the system without the lead.

QD level energy and that the maxima are not generally quantized anymore to $2e^2/h$.

Therefore, a unique signature of MBS is that the two Fano resonances are always mirrored as a function of ε_D at the ordinate, when the coupling to the leads is "local" like in the setup of Fig. 1. This can be explained with the real-valued nature of the Majorana bound states. Because the MBS are described by real-valued spinors, they couple to electron- and hole-like excitations in the same way and $\frac{dI}{dV}(\varepsilon_D) = \frac{dI}{dV}(-\varepsilon_D)$. This result is even valid for finite temperatures and in more realistic setups as we will show explicitly in the next section.

V. KITAEV-CHAIN MODEL

The next step towards an experiment is to consider a one dimensional p -wave superconductor and to discretize its Hamiltonian on a one-dimensional lattice

$$\begin{aligned}
 H_{p\text{-wave}} &= \frac{1}{2} \int dx (\Psi^\dagger(x), \Psi(x)) \begin{pmatrix} -\tilde{t}\partial_x^2 + U & -i2\Delta\partial_x \\ -i2\Delta^*\partial_x & \tilde{t}\partial_x^2 - U \end{pmatrix} \begin{pmatrix} \Psi(x) \\ \Psi^\dagger(x) \end{pmatrix} \\
 &= \sum_{j=1}^N \left(U - \frac{2\tilde{t}}{a^2} \right) \left(c_j^\dagger c_j - \frac{1}{2} \right) \\
 &\quad - \sum_{j=1}^{N-1} \left(\frac{\tilde{t}}{a^2} (c_j^\dagger c_{j+1} + c_{j+1}^\dagger c_j) + \frac{i\Delta}{a} c_j^\dagger c_{j+1}^\dagger + \frac{i\Delta^*}{a} c_j c_{j+1} \right) \\
 &= \frac{i}{2} \sum_{j=1}^N \left(U - \frac{2\tilde{t}}{a^2} \right) \gamma_{2j-1} \gamma_{2j} + \frac{i}{2} \sum_{j=1}^{N-1} \left[\left(\frac{\tilde{t}}{a^2} + \frac{|\Delta|}{a} \right) \gamma_{2j} \gamma_{2j+1} \right. \\
 &\quad \left. + \left(-\frac{\tilde{t}}{a^2} + \frac{|\Delta|}{a} \right) \gamma_{2j-1} \gamma_{2j+2} \right], \tag{21}
 \end{aligned}$$

where $\tilde{t} = \hbar^2/(2m^*)$ and in last step we followed a transformation to Majorana fermions similar as described in Ref. [9]. U plays the role of a chemical potential and can be used to tune the topological properties of the chain [9]. With this Kitaev chain Hamiltonian we can now increase the number of sites while keeping the length $L = Na$ of the wire fixed.

We now couple, with tunneling-amplitude t_2 , a single Dirac-fermionic site (the QD) with energy ε_D and annihilation operator d to the last Dirac-fermionic site (c_N^\dagger) of the chain, and also tunnel-couple the first Dirac-fermionic site of the Kitaev chain (c_1) to the Fermi lead ($\psi^\dagger(0)$) with amplitude t_1 . The total Hamiltonian written in terms of Majorana fermions then reads

$$H = H_{p\text{-wave}} + H_L \tag{22}$$

$$\begin{aligned}
 &+ \frac{i}{2} [-t_2 \gamma_{2N} \gamma_{2N+1} + t_2 \gamma_{2N-1} \gamma_{2N+2} + \varepsilon_D \gamma_{2N+1} \gamma_{2N+2}] \\
 &+ \frac{i}{2} \gamma_1 [(it_1)^* \psi(0) + (it_1) \psi^\dagger(0)] - \frac{i}{2} \gamma_2 [t_1 \psi^\dagger(0) + t_1^* \psi(0)],
 \end{aligned}$$

where we included the QD with the Hamiltonian

$$H_{\text{Dot}} = \varepsilon_D \left(d^\dagger d - \frac{1}{2} \right) = \frac{i}{2} \varepsilon_D \gamma_{2N+1} \gamma_{2N+2}. \tag{23}$$

Without loss of generality, we have chosen t_2 to be real. We implement this Hamiltonian in our full counting statistics formalism and solve the formula for the CGF numerically using Eq. (33). The resulting differential conductance is shown in Fig. 5(a). In the low-energy limit (inset of Fig. 5(a)) we see a good agreement with the effective model (Fig. 1(b)). In the numerical data we see not only the differential conductance peaks which result from Majorana bound states, but also more states inside the spectral p -wave gap ($\Delta_p = 0.1\Gamma$) of the Kitaev chain.

Even calculations at finite temperatures show that the symmetry property of the two Fano resonances in the MBS-QD system are conserved as can be seen in Fig. 5(b). The results from the effective model calculations can be reproduced perfectly.

As a next step we consider again the Kitaev chain and introduce a coupling between the normal conducting Fermi lead and each site and between the QD and each site of the Kitaev chain. We assume that this tunneling is exponentially suppressed with the length of the tunneling distance. With this modification, the tunneling Hamiltonian becomes

$$H_T = \sum_{n=1}^N \left(t_1 e^{-\frac{(n-1)a}{\xi}} \psi^\dagger(0) c_n + t_2 e^{-\frac{(N-n)a}{\xi}} c_n^\dagger d + \text{h.c.} \right), \tag{24}$$

where ξ is the length scale on which the tunneling amplitude decays. In Fig. 6 we present the resulting differential conductance using this tunneling Hamiltonian. When ξ

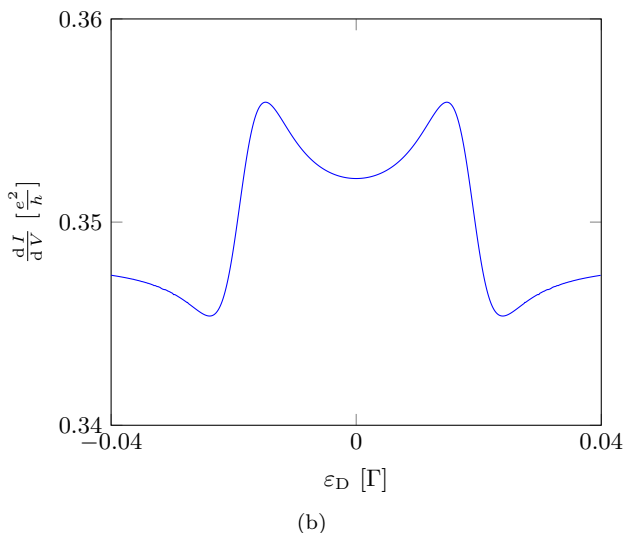
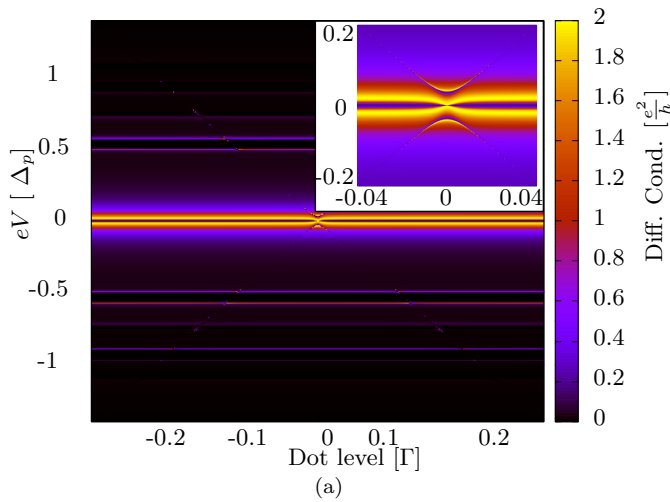


FIG. 5. (a) Differential conductance as function of the dot level energy and the bias voltage between lead and the Kitaev chain with $N = 100$ sites. The parameters are $a = 6 \cdot 10^{-4}$, $\tilde{t} = 1/4500$, $|\Delta| = 1/700$, $\Gamma = 1$, $U = 0.2$ and $t_2 = 0.09$, which corresponds to the topological non-trivial phase. The p -wave gap is around $\Delta_p = 0.1\Gamma$ and above this gap the differential conductance is on the order of $10^{-3} \frac{e^2}{h}$. At lower energies resonances can be seen which correspond to in gap states. The strongest resonance is the Majorana induced resonance with a quantized differential conductance of $\frac{2e^2}{h}$. The influence of the dot can be seen best at the Majorana resonance and results in destructive interference. The inset shows the low energy section. The quantized resonances corresponding to the dot level can not be clearly seen because of resolution problems. (b) Fano resonance at finite temperature $k_B T = 0.01\Delta_p$. This temperature is in agreement with comparable experiments [34]. The symmetry with respect to the dot level energy is conserved also at finite temperatures.

is on the order of the length of the wire the symmetry of the two Fano resonances is broken. However, for $\xi = 0.1L$ the symmetry is restored. We can explain this behaviour by reconsidering the effective model. Here, the symmetry

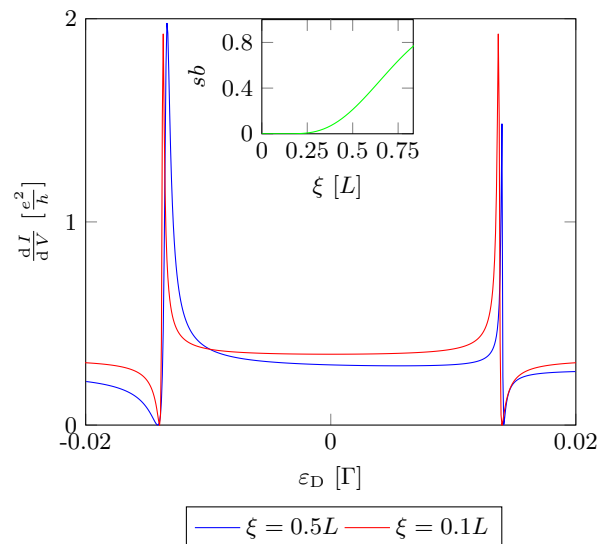


FIG. 6. Fano resonances in the Kitaev chain for non-trivial couplings to normal conducting lead and QD using $t_2 = 0.15\Gamma$. The other parameters are the same as in Fig. 5(a). In the case of long range couplings ($\xi = 0.5L$) the two Fano resonances are no longer symmetric. For a shorter decay length ($\xi = 0.1L$) the symmetry of the two Fano resonances is restored. The inlay shows the symmetry breaking parameter $sb = (p(\varepsilon_D = eV) - p(\varepsilon_D = -eV))/p(\varepsilon_D = eV)$ vs. the tunneling decay length.

is broken if the dot couples to both MBS. We consider the coherence length of the bound states ξ_S which is given in Ref. [9]. In order to couple to both MBS the tunneling decay length needs to be bigger than the difference between the length L of the wire and ξ_S

$$L - \xi_S \ll \xi. \quad (25)$$

The inlay in Fig 6 supports our statement. The symmetry breaking is not visible for all decay length's but starts at a finite value. For our used parameters we find that $\xi_S \approx 0.6L$, which corresponds to the increase in the symmetry breaking parameter

$$sb = \frac{p(\varepsilon_D = eV) - p(\varepsilon_D = -eV)}{p(\varepsilon_D = eV)}. \quad (26)$$

Therefore, this symmetry can be seen as a signature of a single MBS. Because, even if there is a finite overlap between the two MBS and so the ground state is a Dirac-fermionic state the symmetry in ε_D vanishes if and only if both Majorana fermions are contacted.

VII. CONCLUSION

In summary, we studied the resonances in differential conductance and shot noise for the normal conducting lead - Majorana wire - QD setup. We showed that these

resonances, as a function of the QD level energy ε_D , come in pairs and can be described with the Fano-Beutler formula which proves that the observed line-shapes are Fano resonances.

We investigated two models: First, we use an effective low-energy model for the Majorana wire restricting ourselves to hybridized Majorana end states with overlap energy ε . In the case where the lead and the QD are coupled to only one but opposite MBS each, these two Fano resonances are symmetric under $\varepsilon_D \rightarrow -\varepsilon_D$ for all ranges of parameters including finite temperature. At zero temperature, the conductance resonances are always quantized to $2e^2/h$. We also observe a rather striking characteristic that the asymmetry parameter of the Fano resonances changes sign when the bias voltage is tuned through the Majorana fermion overlap energy, a result that is independent on the parameter of the QD giving independent access on the Majorana splitting. In an extended setup where *both* Majorana end states are coupled to the lead and QD, the symmetry of the conductance traces as a function of ε_D is waived and the resonances at zero temperature are not generally quantized anymore.

We support these findings from the effective model calculation by considering a Kitaev chain with a finite length giving us control over the Majorana overlap numerically and find good agreement with the analytical model in the low-energy sector. In particular, we also find asymmetric Fano Resonances when the tunneling between the chain and the lead and between the chain and the QD becomes long range. In this context long means that the tunneling amplitude from the dot and the from lead to the chain needs to reach the MBS at the other side of the chain.

We consider this symmetry in ε_D to be a unique signature of the MBS as it is only lifted if we couple the dot/lead to both MBS and therefore to a non-Majorana fermionic bound state.

We note that the conductance maxima reflecting the spectrum of the MBS-quantum dot system have similarities to a recent experiment in a slightly different setup (not showing Fano resonances), where a quantum dot is coupled to a Fermi lead on one side and a quantum wire on the other [34]. It would be interesting to investigate the role of possible non-local couplings in this setup which should lead to our predicted asymmetries under sign-inversion of the QD level energy ($\varepsilon_D \rightarrow -\varepsilon_D$).

While finishing this manuscript we became aware of two recent related preprints [46, 47] that discuss the energy spectrum of a setup similar to the one in Section IV (without the lead) and note an asymmetry of the spectrum as a function of the QD level energy similar to the maxima in our Fig. 4. However, both preprints do not calculate transport properties.

ACKNOWLEDGMENTS

PR would like to thank Ramón Aguado, Alfredo Levy-Yeyati, Sunghun Park, Elsa Prada, and Pablo San-José for very helpful discussions on this project close to its finalization. We also thank for financial support from the DFG Grant No. RE 2978/1-1, from the Lower Saxony PhD-programme "Contacts in Nanosystems" and the Research Training Group GrK1952/1 "Metrology for Complex Nanosystems", and the Braunschweig International Graduate School of Metrology B-IGSM.

A. Calculation of the CGF

In order to use the following formalism to obtain the CGF we transform the fermionic creation and annihilation operators in terms of Majorana operators. So we rewrite

$$H_M = H_M + H_{Dot} + H_{TDot} \quad (27)$$

$$= \frac{i}{2} \sum_{k,l} A_{kl} \gamma_k \gamma_l. \quad (28)$$

Majorana fermion networks can in general be described by the Hamiltonians

$$H = H_L + H_M + H_T \quad (29)$$

$$H_M = \frac{i}{2} \sum_{k,l} A_{kl} \gamma_k \gamma_l \quad (30)$$

$$H_L = -iv_f \sum_{\alpha} \int dx \psi_{\alpha}^{\dagger}(x) \partial_x \psi_{\alpha}(x) \quad (31)$$

$$H_T = -i \sum_{\alpha\beta} \gamma_{\beta} [t_{\alpha\beta} \psi_{\alpha}^{\dagger}(0) + t_{\alpha\beta}^* \psi_{\alpha}(0)], \quad (32)$$

where γ_k is the real valued creation operator for Majorana bound state k and $A_{kl} = A_{kl}^* = -A_{lk}$, which has to be specified for each setup, H_L describing the leads, where ψ_{α} and ψ_{α}^{\dagger} are the fermionic annihilation and creation operators in lead α and H_T describing the tunnel coupling between the leads and the Majorana fermions. Here v_f is the Fermi velocity and $t_{\alpha\beta}$ is the tunneling amplitude between lead α and Majorana bound state β . We closely follow the derivation of the cumulant generating function using functional integrals provided in [44], which we generalize to arbitrary couplings between normal leads and Majorana fermions and find for the CGF

$$\ln \chi(\vec{\lambda}) = \frac{\mathcal{T}}{2} \int \frac{d\omega}{2\pi} \ln \frac{\det[D^{\lambda}]^{-1}}{\det[D^{\lambda=0}]^{-1}}, \quad (33)$$

where $D^{\lambda}(\omega)$ is the Green's function for the Majorana fermions including the influence of the leads and the counting fields. Its inverse is

$$[D^{\lambda}]^{-1}(\omega) = [D^{(0)}]^{-1}(\omega) - \Sigma^{\lambda}(\omega) \quad (34)$$

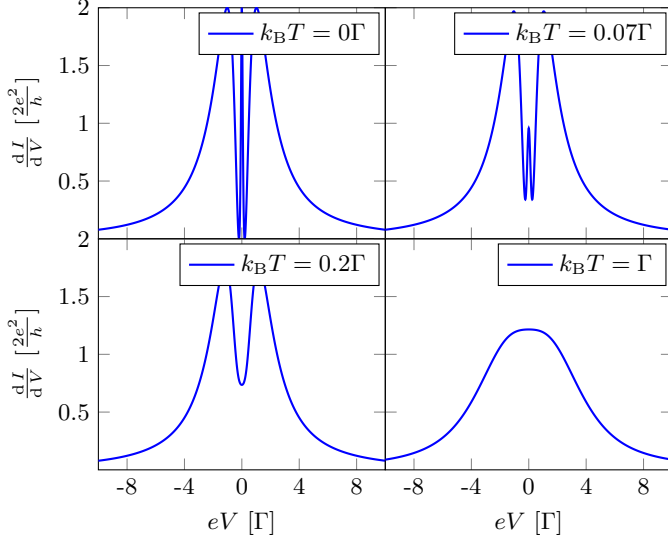


FIG. 7. Differential conductance vs. bias voltage for different temperatures. The parameters for these plots are $\varepsilon = 0.5\Gamma$, $\varepsilon_D = 0.5\Gamma$, $|t_2| = 0.1\Gamma$.

Here $D^{(0)}$ is the unperturbed Majorana Green's function and Σ^λ is the self energy containing the counting fields. The unperturbed Majorana Green's function is defined as $[D^0]_{\alpha\beta}(t, t') = -i \langle T_C \gamma_\alpha(t) \gamma_\beta(t') \rangle$ with T_C the time-ordering operator on the Keldysh contour, and can be calculated using the Heisenberg equation of motion for the free Majorana fermion operators

$$\frac{d\gamma_\alpha}{dt} = i[H_M, \gamma_\alpha] = \sum_\beta 2A_{\alpha\beta}\gamma_\beta, \quad (35)$$

where we used that A is a real skew symmetric matrix. As the unique solutions of Eq. (35) are given by

$$\gamma_\alpha(t) = \sum_\beta \mathcal{B}_{\alpha\beta}(t)\gamma_\beta, \quad (36)$$

with $\mathcal{B}(t) = \exp(2At)$ we can calculate the unperturbed Majorana Green's function $D^{(0)}(t)$. For the calculation of transport properties only energy space properties are used such that we need to consider the Fourier transform of the Majorana Green's function. The inverse of the unperturbed Majorana Green's function in Keldysh matrix representation is given by

$$[D^{(0)}]^{-1}(\omega) = \begin{pmatrix} [D^{(0)}]^{--}(\omega) & 0 \\ 0 & -[D^{(0)}]^{--}(\omega) \end{pmatrix}, \quad (37)$$

where $[D^{(0)}]^{--}(\omega) = iA + \frac{\omega}{2}\mathbb{I}$.

The self energy containing the counting fields is given by

$$\begin{aligned} \bar{\Sigma}_{\alpha\beta}^\lambda(t, t') = & \sum_\delta -t_{\delta\alpha} t_{\delta\beta}^* e^{-i\frac{\lambda_\delta(t) - \lambda_\delta(t')}{2}} G_\delta^{(0)}(t, t') \\ & + t_{\delta\beta} t_{\delta\alpha}^* e^{i\frac{\lambda_\delta(t) - \lambda_\delta(t')}{2}} G_\delta^{(0)}(t', t), \end{aligned} \quad (38)$$

where $G_\delta^{(0)}(t', t)$ is the unperturbed leads Green's function. Its Fourier transform therefore reads

$$\begin{aligned} \Sigma^\lambda(\omega)_{\mu\nu} = & \sum_\alpha \begin{pmatrix} -t_{\alpha\nu} t_{\alpha\mu}^* G_\alpha^{--}(-\omega) & +t_{\alpha\nu} t_{\alpha\mu}^* e^{i\lambda_\alpha} G_\alpha^{+-}(-\omega) \\ t_{\alpha\nu} t_{\alpha\mu}^* e^{-i\lambda_\alpha} G_\alpha^{+-}(-\omega) & -t_{\alpha\nu} t_{\alpha\mu}^* G_\alpha^{++}(-\omega) \end{pmatrix} \\ & + \begin{pmatrix} t_{\alpha\nu} t_{\alpha\mu}^* G_\alpha^{--}(\omega) & -t_{\alpha\nu} t_{\alpha\mu}^* e^{-i\lambda_\alpha} G_\alpha^{+-}(\omega) \\ -t_{\alpha\nu} t_{\alpha\mu}^* e^{i\lambda_\alpha} G_\alpha^{+-}(\omega) & +t_{\alpha\nu} t_{\alpha\mu}^* G_\alpha^{++}(\omega) \end{pmatrix}. \end{aligned} \quad (39)$$

For a constant density of states $\rho_0 = 1/(2\pi v_f)$ inside the leads, the leads Green's function are

$$G_\alpha(\omega) = i2\pi\rho_0 \begin{pmatrix} n_\alpha(\omega) - \frac{1}{2} & n_\alpha(\omega) \\ n_\alpha(\omega) - 1 & n_\alpha(\omega) - \frac{1}{2} \end{pmatrix}. \quad (40)$$

If we now enter this into Eqs. (34) and (33) and calculate the determinant we obtain Eq. (7). Another formalism to obtain the current and noise in the normal - topological superconductor junction using Keldysh Green's functions is given in Ref. [48].

B. Zero Bias Peak (ZBP)

For a finite Majorana overlap $\varepsilon \neq 0$, the conductance at zero bias and temperature vanishes as long as the dot level energy is finite [49]. However, in the case of $\varepsilon_D = 0$ the differential conductance is quantized with $2e^2/h$. At finite temperature, things look different as the temperature reduces the height of the resonances in the differential conductance. It is important to note that the resonance peak corresponding to $\varepsilon_D = 0$ is reduced much faster than the resonances corresponding to the MBS (see Fig. 7).

And for a temperature higher than the Majorana overlap ($k_B T > \varepsilon$) the two peaks are no longer resolved and appear as single ZBP.

-
- [1] E. Majorana, *Nuovo Cimento* **14**, 171 (1937).
 - [2] C. Nayak, S. H. Simon, A. Stern, M. Freedman, and S. Das Sarma, *Rev. Mod. Phys.* **80**, 1083 (2008).
 - [3] J. K. Pachos, "Introduction to topological quantum computation," (Cambridge University Press, 2013).
 - [4] V. Mourik, K. Zuo, S. M. Frolov, S. R. Plissard, E. P. A. M. Bakkers, and L. P. Kouwenhoven, *Science* **336**, 1003 (2012).
 - [5] A. Das, Y. Ronen, Y. Most, Y. Oreg, M. Heiblum, and H. Shtrikman, *Nat. Phys.* **8**, 887895 (2012).
 - [6] E. J. H. Lee, X. Jiang, M. Houzet, R. Aguado, C. M. Lieber, and S. De Franceschi, *Nat. Nanotech.* **9**, 7984 (2013).
 - [7] S. Nadj-Perge, I. K. Drozdov, J. Li, H. Chen, S. Jeon, J. Seo, A. H. MacDonald, B. A. Bernevig, and A. Yazdani, *Science* **346**, 602 (2014).
 - [8] R. Pawlak, M. Kisiel, J. Klinovaja, T. Meier, S. Kawai, T. Glatzel, D. Loss, and E. Meyer, *npj Quantum Information* **2**, 16035 (2016).

- [9] A. Y. Kitaev, *Phys. Usp.* **44**, 131 (2001).
- [10] L. Fu and C. L. Kane, *Phys. Rev. B* **79**, 161408 (2009).
- [11] C. W. J. Beenakker, D. I. Pikulin, T. Hyart, H. Schomerus, and J. P. Dahlhaus, *Phys. Rev. Lett.* **110**, 017003 (2013).
- [12] F. m. c. Crépin and B. Trauzettel, *Phys. Rev. Lett.* **112**, 077002 (2014).
- [13] L. P. Rokhinson, X. Liu, and J. K. Furdyna, *Nat. Phys.* **8**, 795799 (2012).
- [14] J. Wiedenmann, E. Bocquillon, R. S. Deacon, S. Hartinger, O. Herrmann, T. M. Klapwijk, L. Maier, C. Ames, C. Brne, and C. . Gould, *Nat. Comun.* **7**, 10303 (2016).
- [15] S. Das Sarma, M. Freedman, and C. Nayak, *Phys. Rev. Lett.* **94**, 166802 (2005).
- [16] A. Stern and B. I. Halperin, *Phys. Rev. Lett.* **96**, 016802 (2006).
- [17] P. Bonderson, A. Kitaev, and K. Shtengel, *Phys. Rev. Lett.* **96**, 016803 (2006).
- [18] J. Alicea, Y. Oreg, G. Refael, F. von Oppen, and M. P. A. Fisher, *Nat. Phys.* **7**, 412 (2011).
- [19] J. D. Sau, D. J. Clarke, and S. Tewari, *Phys. Rev. B* **84**, 094505 (2011).
- [20] B. van Heck, A. R. Akhmerov, F. Hassler, M. Burrello, and C. W. J. Beenakker, *New J. Phys* **14**, 035019 (2012).
- [21] M. Cheng, R. M. Lutchyn, and S. Das Sarma, *Phys. Rev. B* **85**, 165124 (2012).
- [22] F. L. Pedrocchi and D. P. DiVincenzo, *Phys. Rev. Lett.* **115**, 120402 (2015).
- [23] R. M. Lutchyn, J. D. Sau, and S. Das Sarma, *Phys. Rev. Lett.* **105**, 077001 (2010).
- [24] Y. Oreg, G. Refael, and F. von Oppen, *Phys. Rev. Lett* **105**, 177002 (2010).
- [25] P. W. Brouwer, M. Duckheim, A. Romito, and F. von Oppen, *Phys. Rev. Lett.* **107**, 196804 (2011).
- [26] D. Rainis, L. Trifunovic, J. Klinovaja, and D. Loss, *Phys. Rev. B* **87**, 024515 (2013).
- [27] J. Nilsson, A. Akhmerov, and C. Beenakker, *Phys. Rev. Lett* **101**, 120403 (2008).
- [28] L. Fu, *Phys. Rev. Let.* **104**, 056402 (2010).
- [29] S. M. Albrecht, A. P. Higginbotham, M. Madsen, F. Kuemmeth, T. S. Jespersen, J. Nygård, P. Krogstrup, and C. M. Marcus, *Nature* **531**, 206209 (2016).
- [30] S. Park and P. Recher, *Phys. Rev. Lett.* **115**, 246403 (2015).
- [31] D. E. Liu and H. U. Baranger, *Phys. Rev. B* **84**, 201308 (2011).
- [32] M. Leijnse and K. Flensberg, *Phys. Rev. B* **84**, 140501 (2011).
- [33] E. Vernek, P. H. Penteado, A. C. Seridonio, and J. C. Egues, *Phys. Rev. B* **89**, 115435 (2014).
- [34] M. T. Deng, S. Vaitiekėnas, E. B. Hansen, J. Danon, M. Leijnse, K. Flensberg, J. Nygård, P. Krogstrup, and C. M. Marcus, *Science* **354**, 1557 (2016).
- [35] A. E. Miroshnichenko, S. Flach, and Y. S. Kivshar, *Rev. Mod. Phys.* **82**, 2257 (2010).
- [36] F. A. Dessotti, L. S. Ricco, M. de Souza, F. M. Souza, and A. C. Seridonio, *J. Appl. Phys.* **116**, 173701 (2014).
- [37] J.-J. Xia, S.-Q. Duan, and W. Zhang, *Nanoscale Res. Lett.* **10**, 223 (2015).
- [38] J. Baranski, A. Kobialka, and T. Domanski, *arXiv:1608.02465* .
- [39] Y. Xiong, *Chinese Phys. Lett.* **33**, 057402 (2016).
- [40] A. Ueda and T. Yokoyama, *Phys. Rev. B* **90**, 081405 (2014).
- [41] C. Jiang and Y.-S. Zheng, *Solid State Commun.* **212**, 1418 (2015).
- [42] Q.-B. Zeng, S. Chen, L. You, and R. Lv, *arXiv:1510.06558*.
- [43] L. S. Levitov and M. Reznikov, *Phys. Rev. B* **70**, 115305 (2004).
- [44] L. Weithofer, P. Recher, and T. L. Schmidt, *Phys. Rev. B* **90**, 205416 (2014).
- [45] U. Fano, *Nuovo Cimento* **12**, 154 (1935).
- [46] D. J. Clarke, *arXiv:1702.01740*.
- [47] E. Prada, R. Aguado, and P. San-José, *arXiv:1702.02525*.
- [48] A. Zazunov, R. Egger, and A. Levy Yeyati, *Phys. Rev. B* **94**, 014502 (2016).
- [49] D. I. Pikulin and Y. V. Nazarov, *JETP Letters* **94**, 693 (2012).